# Topological Polymer Dispersed Liquid Crystals with Bulk Nematic Defect Lines Pinned to Handlebody Surfaces

Michael G. Campbell,[1,2] Mykola Tasinkevych,[3,4] and Ivan I. Smalyukh[1,2,5,6,*]
[1]Department of Physics, University of Colorado, Boulder, Colorado 80309, USA
[2]Liquid Crystal Materials Research Center, University of Colorado, Boulder, Colorado 80309, USA
[3]Max-Planck-Institut für Intelligente Systeme, Heisenbergstraße 3, D-70569 Stuttgart, Germany
[4]Institut für Theoretische Physik IV, Universität Stuttgart, Pfaffenwaldring 57, D-70569 Stuttgart, Germany
[5]Department of Electrical, Computer, and Energy Engineering and Materials Science and Engineering Program, University of Colorado, Boulder, Colorado 80309, USA
[6]Renewable and Sustainable Energy Institute, National Renewable Energy Laboratory and University of Colorado, Boulder, Colorado 80309, USA
(Received 18 December 2013; published 16 May 2014)

Polymer dispersed liquid crystals are a useful model system for studying the relationship between surface topology and defect structures. They are comprised of a polymer matrix with suspended spherical nematic drops and are topologically constrained to host defects of an elementary hedgehog charge per droplet, such as bulk or surface point defects or closed disclination loops. We control the genus of the closed surfaces confining such micrometer-sized nematic drops with tangential boundary conditions for molecular alignment imposed by the polymer matrix, allowing us to avoid defects or, on the contrary, to generate them in a controlled way. We show, both experimentally and through numerical modeling, that topological constraints in nematic microdrops can be satisfied by hosting topologically stable half-integer bulk defect lines anchored to opposite sides of handlebody surfaces. This enriches the interplay of topologies of closed surfaces and fields with nonpolar symmetry, yielding new unexpected configurations that cannot be realized in vector fields, having potential implications for topologically similar defects in cosmology and other fields.

DOI: 10.1103/PhysRevLett.112.197801 PACS numbers: 61.30.Jf

Topological defects are key to many physical phenomena and theories [1–12]. Liquid crystal (LC) defects [13] have been used extensively to model the behavior of topologically analogous defects in other physical systems, including cosmic strings in early Universe cosmology [11,12]. On the other hand, LC defects are often undesirable in practical applications such as displays and electro-optic devices, which were driving the exploration of conditions under which topological defects spontaneously appear and annihilate as well as how these can be controlled by fields [14]. Polymer dispersed LCs (PDLCs) have emerged as a technologically important composite system in which defects are inevitable due to spherical droplet confinement of the nematic in the solid polymer matrix [14]. In this system, defects are dictated by topological theorems [15,16] governing interplay between topologies of confining droplet surfaces and nematic director field $\mathbf{n}(\mathbf{r})$, which describes spatially varying local average orientation of anisotropic LC molecules.

In this Letter, we control the topology of closed surfaces confining nematic drops in a polymer matrix. This allows us to either avoid defect formation for drops of genus $g = 1$ or to generate defects of well-defined type in drops of $g > 1$, giving origins to topological PDLCs (TPDLCs). By means of three-dimensional (3D) nonlinear optical imaging [17] and numerical minimization of the Landau–de Gennes free energy [13,14], we show that the nontrivial confinement geometry and topology of drops [18–22] prompt the formation of topologically stable line defects that cross the entire handlebody-shaped volume and pin to surfaces with tangential boundary conditions. This is in strong contrast to what occurs in spherical nematic drops [14], in large millimeter-sized drops with handles [24], and in all physical fields in contact with closed surfaces of different genus probed so far [15]. Using simple analytical energetic and topological analysis, we explain observed director and defect configurations and how they are selected from a host of possible ways of satisfying topological constraints dictated by mathematical theorems. This is consistent with numerical modeling, providing insights into how new topology-controlled structures in TPDLCs can be used in applications and as model systems.

To create TPDLCs, we first fabricated handlebody-shaped silica microstructures using photolithography [16]. Norlin Optical Adhesive (NOA63) was then squeezed with the substrate containing these silica microstructures. Desired micrometer-sized polymer confinement structures were then obtained using replica molding [18]. The polymer was cured using the OmniCure S2000 illumination system (Lumen Dynamics) by high-intensity 320-to 400-nm UV radiation for 15–30 seconds. After curing, the polymer sheet was peeled off to leave the desired surface topography

 

on one of its sides. We also fabricated flat thin polymer microfilms by curing NOA63 between two flat substrates at the same illumination. To create TPDLC films containing nematic drops, we infiltrated a room-temperature nematic mixture E31 (from EM Chemicals) into a gap between a flat polymer sheet and the film with microstructures and pressed the two together as well as sealed by additional UV curing. This procedure yields polymer films containing LC drops with $g = 1$–5 and with rounded-square cross sections [16].

3D imaging was performed with three-photon excitation fluorescence polarizing microscopy (3PEF-PM) based on an inverted microscope IX 81 (Olympus), a tunable Ti-sapphire oscillator (680–1080 nm, Coherent) emitting 140-fs pulses at a repetition rate of 80 MHz, an oil-immersion ×100 objective with a numerical aperture of 1.4, and a photomultiplier tube detector H5784-20 (Hamamatsu) [17]. Submicron resolution along the microscope's axis was enabled by the nonlinear nature of optical excitation. The detected 3PEF-PM intensity exhibited a strong ($\propto \cos^6\theta$) dependence on the angle $\theta$ between $\mathbf{n}(\mathbf{r})$ and the linear polarization of excitation light, allowing reconstruction of complex $\mathbf{n}(\mathbf{r})$ inside the drops [17,19]. Using 3PEF-PM images obtained for different polarizations of excitation light, we have constructed 3D representations of nematic field configurations and defects. We also probed $\mathbf{n}(\mathbf{r})$ by a conventional polarizing optical microscopy (POM) [14]. TPDLCs were modeled by numerical minimization of the Landau–de Gennes free energy [20] with an additional tangentially degenerate surface anchoring term [21]. The total free energy was then minimized numerically for experimental material and geometric parameters [22], as described in the Supplemental Material [23].

Figure 1 shows an array of torus-shaped drops of $g = 1$ suspended in a polymer matrix. Most of them contain defect-free concentric $\mathbf{n}(\mathbf{r})$, as expected for the confinement surface with Euler characteristic $\chi = 2 - 2g = 0$. Interestingly, unlike in millimeter-large $g = 1$ drops [24], our field configurations contain no detectable double twist (Fig. 1) that could potentially originate from the saddle-splay term of free energy. We attribute this to the rounded-square cross section of the torus that hinders formation of double-twist configurations, which are incompatible with the square cross section because additional distortions would have to be introduced to accommodate such structures. In addition to defect-free configurations, droplets containing pairs of self-compensating defects [Figs. 1(a) and 1(b)] are occasionally observed too, in agreement with numerical calculations [Figs. 1(f)–1(h)].

Nematic drops with $g > 1$ are expected to host topological defects [15]. The Poincare-Hopf theorem [15] requires that the winding number $s$ of defects at the LC-polymer interface adds to $s = \chi = 2 - 2g$, where $s$ is defined as the number of times $\mathbf{n}(\mathbf{r})$ rotates around the two-dimensional defect as one circumnavigates it once.

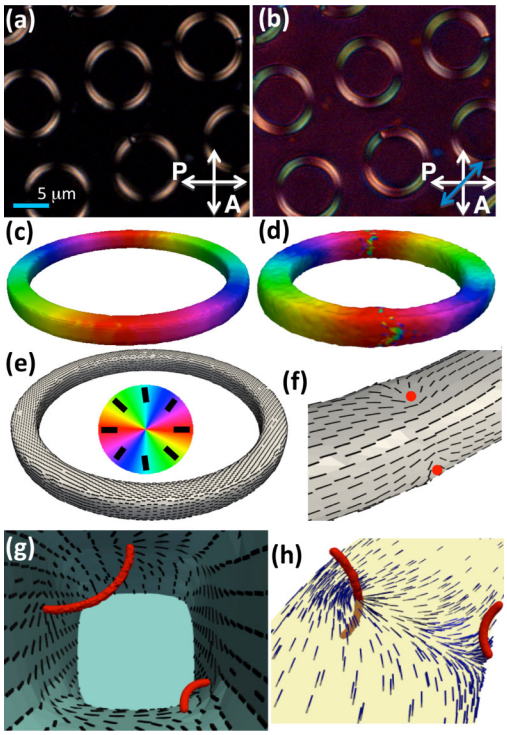


FIG. 1 (color online). TPDLC with $g = 1$ nematic drops. (a) and (b) POM micrographs obtained (a) without and (b) with an additional phase retardation plate. Polarizer and analyzer orientations are shown using white double arrows, and the slow axis of the phase retardation plate is shown by a blue double arrow. (c) and (d) 3D representation of $\mathbf{n}(\mathbf{r})$ at the surface of a $g = 1$ drop based on (c) numerical modeling and (d) experiments, with the color-coded scheme of azimuthal orientations shown in the inset of (e). (e) Computer-simulated $\mathbf{n}(\mathbf{r})$ of a defect-free equilibrium configuration. (f)–(h) $\mathbf{n}(\mathbf{r})$ in the vicinity of self-compensating defects found in metastable states of some drops as depicted (f) at the LC-polymer interface, (g) in drop's interior, and (h) in a plane intersecting the defect lines. Disclinations are shown as red tubes and filled circles representing regions of reduced scalar order parameter.

However, topological theorems do not prescribe particular ways in which this constraint should be satisfied, e.g., by means of point or line defects or through the defects of a particular $s$. Furthermore, the LC director has a nonpolar symmetry allowing half-integer $s$ of defects, enriching the interaction between topologically nontrivial closed surfaces and $\mathbf{n}(\mathbf{r})$ as compared to that of vector fields. Minimization of the total free energy of drops is a mechanism of selecting stable and metastable states from a host of configurations satisfying topological constraints. Global and local minima of the free energy correspond to topologically constrained structures found in TPDLC drops. In high-genus drops, most defects, especially the ones required by topology, tend to localize in junction regions between tori (Figs. 2–4). What is interesting is that, unlike in the case of much larger drops with handles [24], we observe no boojums (surface point defects), but rather half-integer line defects spanning

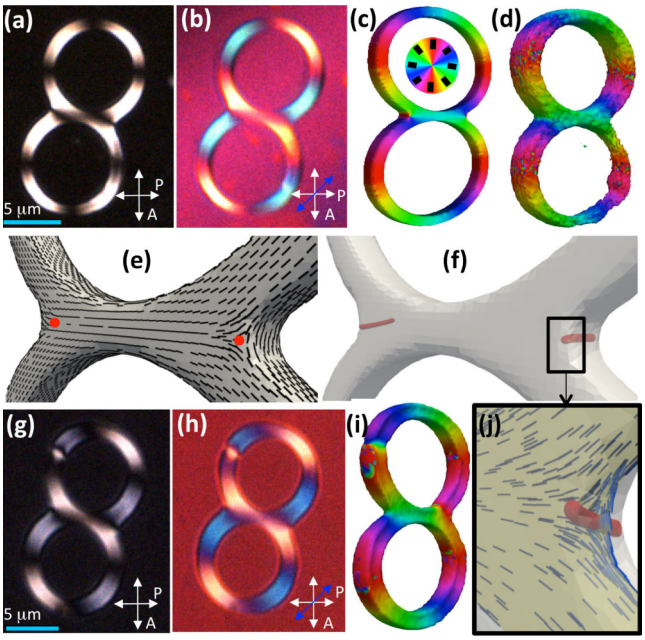


FIG. 2 (color online). Nematic $g = 2$ drops. (a) and (b) POM micrographs obtained (a) without and (b) with an additional phase retardation plate. (c) and (d) 3D representation of $\mathbf{n}(\mathbf{r})$ at the surface of a $g = 2$ drop based on (c) numerical modeling and (d) experiments. The color-coded scheme of azimuthal orientations is shown in the inset of (c). (e) and (f) Nematic configurations and defects at the junction of two tori, with (e) $\mathbf{n}(\mathbf{r})$ at the LC-polymer interface depicted using rods and the line defect cores in the bulk of the $g = 2$ drop shown using regions of reduced scalar order parameter. (g) and (h) A metastable configuration with a pair of additional self-compensating defects probed using POM (g) without and (h) with an additional phase retardation plate. (i) The corresponding experimental 3D representation of $\mathbf{n}(\mathbf{r})$ at the surface of a $g = 2$ drop. (j) $\mathbf{n}(\mathbf{r})$ in the vicinity of a defect in a midplane of a $g = 2$ drop.

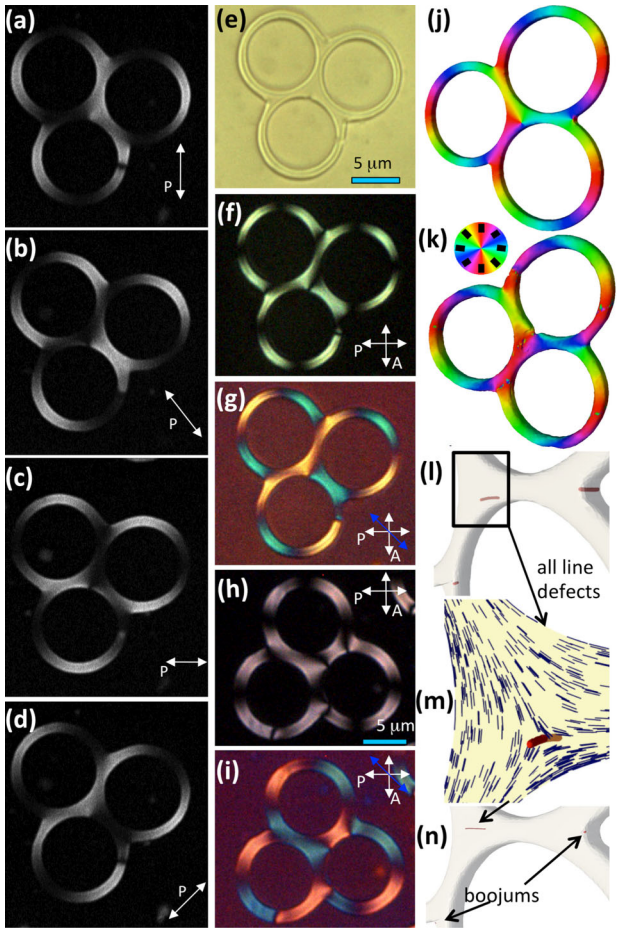


FIG. 3 (color online). Nematic $g = 3$ drops. (a)–(d) 3PEF-PM images obtained for a midplane of the handlebody-shaped drops at different linear polarizations of excitation light (white double arrows). (e–i) Optical micrographs of two different $g = 3$ drops obtained (e) without polarizers, (f) and (h) between crossed polarizers, and (g) and (i) between crossed polarizers and with an additional phase retardation plate. (j) and (k) 3D representations of $\mathbf{n}(\mathbf{r})$ at the LC-polymer interface obtained (j) by numerical modeling and (k) experimentally; the color-coded scheme of azimuthal orientations is shown in the inset. (l) and (m) Defect lines at tori junctions and (m) $\mathbf{n}(\mathbf{r})$ shown for one of them. (n) Co-existence of a line defect at the triple junction with boojums in other locations of a larger drop. The red tubelike defect regions are defect cores with reduced scalar order parameter.

through the entire thickness of drops. This can be seen, for example, by taking depth-resolved 3PEF-PM cross sections at different directions of linearly polarized excitation light [Figs. 3(a)–3(d)]. Similar evidence is provided by both experimental and numerically simulated color-coded 3D representations of $\mathbf{n}(\mathbf{r})$ shown in Figs. 2(c), 2(d), 2(i), 3(j), 3(k), 4(b), 4(c), and 4(j), which indicate the presence of line defects ending at opposite sides of drops. By varying perspective views on such 3D representations, we confirm that defects in the intertori junctions are all half-integer singular lines pinned to opposite handlebody surfaces (being topologically stable defect lines, they cannot interrupt in the LC bulk). Some of the drops contain the minimum numbers of half-integer defects needed to satisfy topological constraints on the net winding number $s = \chi$. For example, $g = 2$ drops tend to have two $s = -1/2$ bulk defect lines spanning the droplet's thickness [Figs. 2(a)–2(f)]. Drops with $g = 3$ have at least four such defects (Fig. 3); $g = 4$ drops have at least six, and $g = 5$ drops have at least eight disclinations in the junction region (Fig. 4).

In addition to topologically required ones, pairs of self-compensating defect lines often appear [Figs. 2(g)–2(i)]. These additional self-compensating pairs of defects [depicted in Figs. 1(f)–1(h) by thin red tubes with reduced scalar order parameter] connect flat regions of surfaces of the rounded-square cross sections at 90° with respect to each other. Such defect lines would have to extend in length to annihilate, which would increase their energetic cost up until annihilation, resulting in their metastability. Neglecting differences in Frank elastic constants, their line tension (free energy per unit length) can be estimated as $T_d = (\pi/4)K \ln(L/r_{\text{core}}) + T_{\text{core}}$

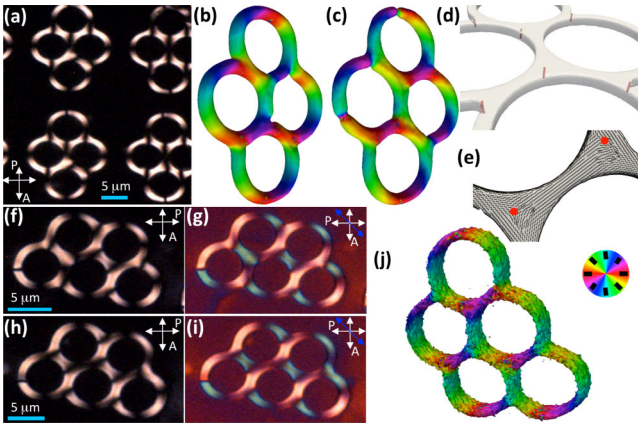


FIG. 4 (color online). Nematic $g = 4$ and $g = 5$ drops. (a) POM micrograph and (b) and (c) 3D $\mathbf{n}(\mathbf{r})$ for two different $g = 4$ drops. (d) and (e) the corresponding numerical results depicting (d) defect lines in the junction regions and (e) $\mathbf{n}(\mathbf{r})$ at the LC-polymer interface, with two defect lines marked by red filled circles. (f)–(i) POM micrographs showing two different $g = 5$ drops obtained (f) and (h) without and (g) and (i) with an additional phase retardation plate. (j) 3D representation of $\mathbf{n}(\mathbf{r})$ of a $g = 5$ drop; the color-coded scheme of azimuthal orientations is shown in the inset.

[13,20], where $K$ is an average elastic constant, $L$ is the system size, $r_{\text{core}}$ and $T_{\text{core}}$ are the radius and energy of the defect core. Assuming an isotropic (melted) core, $T_{\text{core}} = \pi K/4$ and $r_{\text{core}} \sim 10\,\text{nm}$. For $K = 10$ pN, one finds $T_d = (60\text{–}75)$ pN. Stretching such a defect line by 100 nm increases free energy by $\sim 10^{-17}$ J, much larger than thermal energy at room temperature so that the defect annihilation within these pairs cannot be thermally activated. Self-compensating defect lines are bent toward each other as arches in diametrically opposite corners of the square cross section [Figs. 1(f)–1(h)], which is because of the competition between the energetic cost of extending defect lengths and the energetic benefit of reducing strong elastic distortions in between the defect lines of opposite $s$. Within the self-compensating pairs, the shorter and longer defects have winding numbers of $s = -1/2$ and $s = 1/2$, respectively [Fig. 1(g)]. This is caused by their different line tensions and surface energies associated with the mismatch between their bulk field distributions and boundary conditions. By quenching the samples from isotropic phase multiple times in both experiments and modeling, we have verified that the location of defects is not linked to surface imperfections. Although many defects appear immediately following a temperature quench as the system cools from the isotropic to nematic phase, most of them annihilate, leaving the topologically required ones, with occasional metastable structures [Figs. 1(f)–1(h)].

Only point defects, including surface boojums and bulk hedgehogs, or closed disclination loops topologically equivalent to them have been observed and modeled theoretically in $g \geq 0$ nematic drops [24–27]. We show that closed $g > 1$ surfaces can also generate topology-satisfying defect lines pinned to opposite sides of droplet surfaces and running through their bulk. These findings show equivalence of surface-pinned line defects and boojums in such confinement geometries. In principle, topological constraints in spherical drops with tangential anchoring could be also satisfied by half-integer droplet-crossing disclinations with ends pinned to surfaces, but such structures have never been observed due to their high energetic cost. For $g > 1$, however, defect lines are key to realizing equilibrium structures and have well-defined locations in intertori junctions [Figs. 2(e), 2(f), 2(j), 3(l), 3(m), 4(d), and 4(e)]. Their appearance is unrelated to the core structure of point defects as the size of such ringlike cores [22] is of the order of a coherence length (~15 nm). Our bulk-crossing defect lines are observed in experimental and numerical minimum-energy structures for $g > 1$ drops with the size of 65–1000 nematic coherence lengths. In the largest 15-$\mu$m droplets that we studied, boojums and half-integer defect lines coexist because they correspond to lower free energy depending on locations of these defects within the drops. For example, the defect lines going through the central junctions of $g = 3$ handlebody [Fig. 3(m)] are stable even in these drops while other defects transform to boojums [Fig. 3(n)]. Certainly, if the droplet size increases to the millimeters [24], one can expect that only boojums would be stable because of the lower free energy of structures to which they correspond (although half-integer defect lines may still be found as metastable states).

Although the Poincare-Hopf theorem predicts defects in fields on closed surfaces, implications of the nonpolar nature of $\mathbf{n}(\mathbf{r})$ as compared to vector fields remained unknown. Prior studies of millimeter-sized drops seemed to indicate that it might be inconsequential, as the observed boojums had integer $s$, as expected for vector fields. We show that the nonpolar nature of $\mathbf{n}(\mathbf{r})$ allows for satisfying topological theorems in an entirely different way, through the appearance of half-integer defect lines, a scenario that cannot be realized in media with vector fields and that (surprisingly) has never been considered experimentally or theoretically. This may have important implications for other branches of science, where fields are also nonpolar but experimental insights are less available (e.g., cosmic strings are topologically similar to nematic defect lines of $s = \pm 1/2$). It was the microconfinement that led to this finding because these novel structures with half-integer defects are energetically unstable in millimeter-sized droplets explored before [24].

Soft lithography allows for mass fabrication of TPDLCs. By forming multilayer films, one may design TPDLCs with 3D-periodic arrays of topologically nontrivial drops. In addition, holographically guided polymer-LC phase separation during polymerization may be also used to form droplet structures with $g \geq 1$ in a scalable manner [14]. On the other hand, two-photon photopolymerization may be exploited to obtain drops with even more

sophisticated surface topology, such as freestanding knots, links, Seiphert surfaces, and Möbius strips and shells formed by them [1,28–30], thus opening a new experimental playground for low-dimensional topology in physical systems. TPDLC drops can be fabricated to have one surface exposed to polar fluids such as water, thus potentially expanding the spectrum of LC-based techniques used for chemical and biological detection [31–33].

To conclude, we developed PDLCs with topologically nontrivial shapes of drops, dubbed "TPDLCs." By controlling genus of confining surfaces, we showed that defects in TPDLC drops can be avoided for $g = 1$, and the net topological winding number of defects can be controlled for $g > 1$. Out of all topology-satisfying field and defect configurations, free energy of the system selects half-integer defect lines spanning through the LC bulk. This behavior is very different from that observed in spherical drops and in large millimeter-sized drops with handles [24]. Future studies will address the role of chirality in defining TPDLC director field and defect configurations, as well as how these structures can be controlled by means of electric and optical switching of $\mathbf{n}(\mathbf{r})$ as well as by reducing the droplet size to nanometer scales. It will be of interest to extend the topology of confining surfaces to that of knots and various nonorientable surfaces [15], such as Möbius strips. From a practical standpoint, topological constraints on nematic fields may allow for bistable modes of electric switching of TPDLCs.

We acknowledge discussions with M. Bowick, Q. Liu, T. Lubensky, and B. Senyuk. We thank Q. Liu for fabricating silica microstructures that we used as replicas. This work was supported by NSF Grant No. DMR-0847782 (M. G. C. and I. I. S.) and partially by the FP7 IRSES Marie-Curie Grant No. PIRSES-GA-2010-269181 (M. T.).

*To whom all correspondence should be addressed.
ivan.smalyukh@colorado.edu

[1] L. H. Kauffman, *Knots and Physics* (World Scientific Publishing, Singapore, 2000), 3rd ed.
[2] V. A. Rubakov and M. E. Shaposhnikov, Phys. Lett. **125B**, 136 (1983).
[3] A. Vilenkin and E. P. S. Shellard, *Cosmic Strings and Other Topological Defects* (Cambridge University Press, Cambridge, 1994).
[4] H. J. De Vega, I. M. Khalatnikov, and N. G. Sanchez, *Phase Transitions in the Early Universe: Theory and Observations* (Kluwer Academic Publishers, Dordrecht, Netherlands, 2001).
[5] L. Faddeev and A. J. Niemi, Nature (London) **387**, 58 (1997).
[6] Q. Liu, B. Senyuk, M. Tasinkevych, and I. I. Smalyukh, Proc. Natl. Acad. Sci. U.S.A. **110**, 9231 (2013).
[7] R. V. Buniy and T. Kephart, Int. J. Mod. Phys. A **20**, 1252 (2005).
[8] T. Araki, M. Buscaglia, T. Bellini, and H. Tanaka, Nat. Mater. **10**, 303 (2011).
[9] M. R. Dennis, R. P. King, B. Jack, K. O'Holleran, and M. J. Padgett, Nat. Phys. **6**, 118 (2010).
[10] D. M. Kleckner and W. T. Irvine, Nat. Phys. **9**, 253 (2013).
[11] I. Chuang, R. Durrer, N. Turok, and B. Yurke, Science **251**, 1336 (1991).
[12] M. J. Bowick, L. Chandar, E. A. Schiff, and A. M. Srivastava, Science **263**, 943 (1994).
[13] P. M. Chaikin, and T. C. Lubensky, *Principles of Condensed Matter Physics* (Cambridge University Press, Cambridge, 2000).
[14] G. P. Crawford and S. Žumer, *Liquid Crystals in Complex Geometries Formed by Polymer and Porous Networks* (Taylor and Francis, London, 1996).
[15] J. W. Milnor, *Topology from the Differentiable Viewpoint* (The University Press of Virginia, Charlottesville, 1965).
[16] B. Senyuk, Q. Liu, S. He, R. D. Kamien, R. B. Kusner, T. C. Lubensky, and I. I. Smalyukh, Nature (London) **493**, 200 (2013).
[17] R. P. Trivedi, T. Lee, K. A. Bertness, and I. I. Smalyukh, Opt. Express **18**, 27658 (2010).
[18] Y. Xia and G. M. Whitesides, Angew. Chem., Int. Ed. Engl. **37**, 550 (1998).
[19] B. G. Chen, P. J. Ackerman, G. P. Alexander, R. D. Kamien, and I. I. Smalyukh, Phys. Rev. Lett. **110**, 237801 (2013).
[20] P. G. de Gennes and J. Prost, *The Physics of Liquid Crystals* (Clarendon, Oxford, 1993), 2nd ed.
[21] J. B. Fournier and P. Galatola, Europhys. Lett. **72**, 403 (2005).
[22] M. Tasinkevych, N. M. Silvestre, and M. M. Telo da Gama, New J. Phys. **14**, 073030 (2012).
[23] See Supplemental Material at http://link.aps.org/supplemental/10.1103/PhysRevLett.112.197801 for the details of numerical modeling.
[24] E. Pairam, J. Vallamkondu, V. Koning, B. C. van Zuiden, P. W. Ellis, M. A. Bates, V. Vitelli, and A. Fernandez-Nieves, Proc. Natl. Acad. Sci. U.S.A. **110**, 9295 (2013).
[25] D. L. Stein, Phys. Rev. A **19**, 1708 (1979).
[26] G. E. Volovik, Pis'ma Zh. Eksp. Teor. Fiz. **28**, 65 (1978) [JETP Lett. **28**, 59 (1978)].
[27] G. E. Volovik and O. D. Lavrentovich, Pis'ma Zh. Eksp. Teor. Fiz. **85**, 1159 (1983) [JETP Lett. **58**, 1159 (1983)].
[28] A. Martinez, M. Ravnik, B. Lucero, R. Visvanathan, S. Žumer, and I. I. Smalyukh, Nat. Mater. **13**, 258 (2014).
[29] D. Seč, S. Čopar, and S. Žumer, Nat. Commun. **5**, 3057 (2014).
[30] G. P. Alexander, B. G. Chen, E. A. Matsumoto, and R. D. Kamien, Rev. Mod. Phys. **84**, 497 (2012).
[31] S. J. Woltman, D. G. Jay, and G. P. Crawford, Nat. Mater. **6**, 929 (2007).
[32] G. M. Koenig, I.-H. Lin, and N. L. Abbott, Proc. Natl. Acad. Sci. U.S.A. **107**, 3998 (2010).
[33] I.-H. Lin, D. S. Miller, P. J. Bertics, C. J. Murphy, J. J. de Pablo, and N. L. Abbott, Science **332**, 1297 (2011).